Optics Letters

Visible photon generation via four-wave mixing in near-infrared near-zero-index thin films

Enrico G. Carnemolla,[1] Wallace Jaffray,[1] Matteo Clerici,[2] Lucia Caspani,[3] Daniele Faccio,[4] Fabio Biancalana,[1] Clayton Devault,[5] Vladimir M. Shalaev,[5] Alexandra Boltasseva,[5] and Marcello Ferrera[1,*]

[1]Institute of Photonics and Quantum Sciences, Heriot-Watt University, SUPA, Edinburgh EH14 4AS, UK
[2]James-Watt School of Engineering, University of Glasgow, Glasgow G12 8QQ, UK
[3]Institute of Photonics, Department of Physics, University of Strathclyde, Glasgow G1 1RD, UK
[4]School of Physics and Astronomy, University of Glasgow, Glasgow G12 8QQ, UK
[5]Department of Physics & Astronomy and Birck Nanotechnology Center, Purdue University, West Lafayette, Indiana 47907, USA
*Corresponding author: m.ferrera@hw.ac.uk

Received 15 June 2021; revised 13 September 2021; accepted 13 September 2021; posted 17 September 2021 (Doc. ID 433834); published 28 October 2021

Optical nonlinearities can be strongly enhanced by operating in the so-called near-zero-index (NZI) regime, where the real part of the refractive index of the system under investigation approaches zero. Here we experimentally demonstrate semi-degenerate four-wave mixing (FWM) in aluminum zinc oxide thin films generating radiation tunable in the visible spectral region, where the material is highly transparent. To this end, we employed an intense pump (787 nm) and a seed tunable in the NIR window (1100–1500 nm) to generate a visible idler wave (530–620 nm). Experiments show enhancement of the frequency conversion efficiency with a maximum of 2% and a signal-to-pump detuning of 360 nm. Effective idler wavelength tuning has also been demonstrated by operating on the temporal delay between the pump and signal.

https://doi.org/10.1364/OL.433834

Integrated nonlinear systems have the ambitious goal of efficiently manipulating light with light on subwavelength optical paths [1]. To this end, parametric processes are key for coherent light generation at wavelengths not easily accessible via direct material engineering while also being particularly relevant in the domain of quantum optics [2]. However, all-optical integrated systems must overcome outstanding challenges to have an impact on real-life applications (e.g., scalability issues and weak nonlinearities). Promising results have been recently reported using transparent conducting oxides (TCOs) [3,4]. These are hybrid compounds attained by extreme doping of wide-bandgap materials for which the enhanced carrier concentration (typically of the order of 10^{21} cm^{-3}) pushes the Fermi level up into the conduction band, thus effectively widening the natural energy gap of the intrinsic material via Moss–Burstein shift. In this way, both electrical conductivity and optical transparency can be enhanced at the same time [5]. In addition to being optically tunable, CMOS compatible, and relatively transparent, these materials allow access to the so-called near-zero-index (NZI) regime at telecom wavelengths in their bulk form, where the material nonlinearities have been shown to be significantly enhanced [6–13]. A rigorous analysis performed on the dispersive properties of TCOs revealed a low group velocity near its NZI region, the origins of which can be understood from Eq. (1) below

$$v_g = \frac{c\sqrt{\varepsilon(\omega)}}{\varepsilon(\omega) + \frac{\omega}{2}\frac{\mathrm{d}\varepsilon(\omega)}{\mathrm{d}\omega}}. \tag{1}$$

The low group velocity leads to slow light effects similar to other systems such as photonic crystals and micro-cavities [14–18]. However, TCOs have several relevant practical advantages over other nonlinear systems, such as a reduced effective propagation distance and ease of fabrication. It is, however, essential to point out that fundamental differences remain between structured slow light and material slow light [19]. For instance, while the former case is typically accompanied by a field enhancement, the latter is not. We should also underline that in our materials both permittivity and index approach zero in the near-infrared region (NIR). These two conditions are not equivalent but are both at the base of a plethora of interesting effects and enhanced nonlinearities [20–25]. As said, we should always keep in mind that operating at the wavelength where the material's real permittivity vanishes (epsilon-near-zero region) is insufficient to guarantee a correspondent near-zero index.

Up to now, $\chi^{(3)}$ processes in NZI media have mainly been investigated around degeneracy in the infrared part of the spectrum [26,27]. Research efforts have also been made to exploit alternative ENZ materials in the visible (VIS) spectral range [28,29]. However, only organic thin films have produced relevant nonlinear results with acceptable transparency [30].

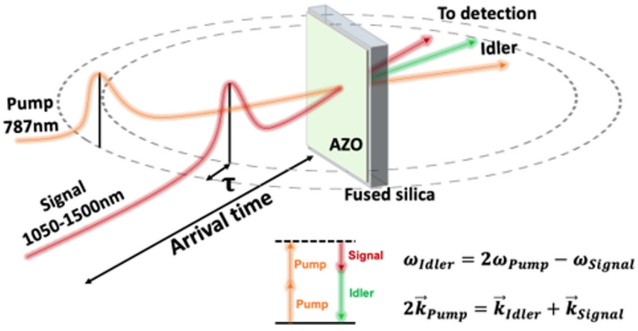

Fig. 1. Schematics of the semi-degenerate four-wave mixing process in aluminum zinc oxide (AZO) thin films. The sketch represents the out-of-plane configuration used for the experiments plus the tunable temporal delay between pump and signal. The inset at the bottom reports the simplified energy diagram and conditions for energy and momentum conservation.

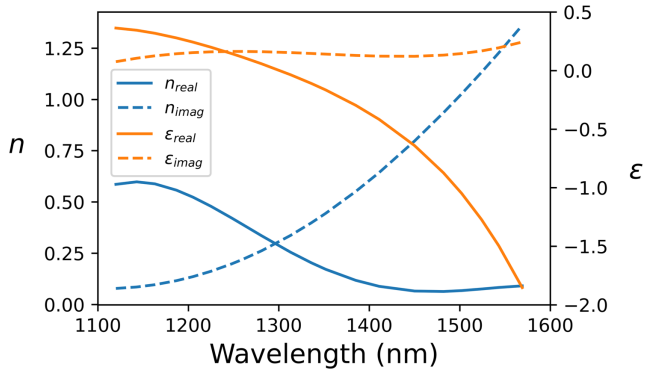

Fig. 2. Refractive index (blue) and relative permittivity (orange) of AZO film. Data recovered via inverse transfer matrix method.

In this Letter, we report on semi-degenerate four-wave mixing (FWM), [$2\omega_p = \omega_s + \omega_i$; the degeneracy only involves the two photons from the pump wave (see Fig. 1)] in aluminum zinc oxide (AZO) thin films ($\lambda_{NZI} \approx 1350$ nm) leading to the generation of idler frequencies in the VIS range. During the process, two pump photons are converted into an amplified signal and an idler photon inside the AZO thin film, according to the energy conservation rule shown in the inset of Fig. 1 [31]. Momentum conservation also constrains the FWM process, resulting in optimal conversion efficiencies when phase matching is fulfilled: $\vec{2}k_p = \vec{k}_s + \vec{k}_i$, which relaxes, in the case of subwavelength films, to the condition of transverse momentum conservation: $\vec{k}_i = -\vec{k}_s$ (where we have considered that the pump impinges on the thin film at normal incidence). The FWM process reported here is of particular technological relevance because TCOs possess very high transparency in the VIS window and idler photons are entirely available for signal processing when coherence preservation is a fundamental concern (e.g., for manipulating quantum states). In addition to this, the FWM process is also attractive for the design of compact tunable sources [32] and potential integration with other emerging material platforms operating in the VIS-NIR wavelength ranges (e.g., perovskites [33]).

Our results show that, for a pump-to-signal wavelength detuning of about 360 nm, the external conversion efficiency η_{ext} of the FWM process, here defined as the ratio between external idler and seed signal intensities, $\eta_{ext} = I_{i,ext}/I_{s,ext}$, exhibits a threshold-like behavior with a steep rising gradient (3%/100 nm). Even though characterization of the nonlinear process was not possible at wavelengths below 1 μm, due to the limited tunability range of the optical parametric amplifier (OPA) in use, the high efficiency gradient makes the experimental configuration used in our work of practical interest. It is worth noting that the experimentally demonstrated 2% conversion efficiency is already potentially useful for those applications where high-power idler signals are not required, such as spectroscopy. The pump and probe experiments also allowed for investigating how the idler spectrum is affected by the pump-to-signal delay. We note that the time-dependent change in the material refractive index induced by the pump pulse was sufficient to shift the idler spectrum by 24 nm on average, as the signal swipe in time the pump. The frequency detuning attained in this way was larger than the idler bandwidth, thus providing an interesting route for ultra-fast optical routing.

Experiments have been conducted on a 900-nm-thick AZO film deposited on a fused silica substrate, the latter ensuring a negligible nonlinear contribution as proven during the experiment calibration procedures. The AZO film was deposited on the silica substrate by pulsed laser deposition. Fabrication details can be found in [34]. The complex refractive index and permittivity were calculated by fitting reflectance and transmission data, calculated through a transfer matrix approach, with experimental reflection and transmission data (see Fig. 2). A few factors determined the choice of AZO over other TCOs: (i) higher electron mobility and lower optical losses at telecom wavelengths [35,36]; (ii) ease of fabrication [34,37]; and (iii) sustainability (AZO is not composed of rare elements such as indium) [38]. In addition to these desirable features, AZO (as most of the ZnO-based TCOs), also exhibits remarkable piezoelectric, pyro-electric, and piezo-optic properties, which makes it very versatile for the fabrication of different nanodevices with multiple functionalities [39,40]. The experiment relied on a standard pump and probe setup (see Fig. 3), where the pump signal was delivered by a Ti:sapphire laser emitting 110 fs pulses with a repetition rate of 100 Hz. Part of the pump is used to feed an OPA that generates the tunable signal wave (1050–1500 nm). Pump and signal propagate along two different optical paths before being spatially overlapped and focused onto the AZO sample. Both pump and signal impinge the film at approximately normal incidence (<10°). A motorized stage regulates the time delay τ between pump and probe with femtosecond precision.

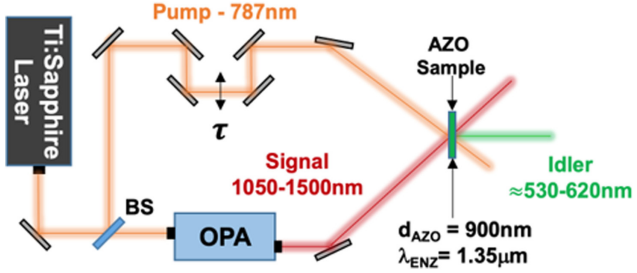

Fig. 3. FWM Experimental setup. A pump beam at 787 nm amplifies a tunable signal (1050–1500 nm) in a highly nonlinear thin AZO film. Idler photons are generated in the visible range (≈530–620 nm) according to energy conservation. A delay line allows for studying the process dynamics.

The pump-to-signal waist ratio was set to 5:1, while operational fluences for pump and signal beams were 37 mJ/cm^2 and 10 mJ/cm^2, respectively. Idler spectra were recorded with a compact spectrometer (Ocean Optics) calibrated in spectral power density. In Fig. 4, we show the most relevant graphs pertaining to the performance of the FWM process investigated. Experiments show low conversion efficiency (<0.1%) for signal wavelength larger than 1150 nm. The maximum conversion efficiency was measured to be about 2% within the signal wavelength range provided by the OPA, with no sign of saturation. The limited OPA range restricts the bandwidth over which the idler radiation is generated with high efficiency within nearly 80 nm (see blue area Fig. 4). It is important to note that broadband ellipsometry measurements point toward a further increase in the efficiency for signal-to-pump wavelengths detuning over experimental capacity. Since a direct evaluation of $\chi^{(3)}$ would be experimentally problematic, the monotonic behavior reported in Fig. 4 is instead investigated by fitting the Eq. (2) to our experimentally retrieved η_{ext} [41]

$$\eta_{\text{ext}} = \frac{I_{i,\text{ext}}}{I_{s,\text{ext}}} = T_i T_s T_p{}^2 \frac{9(\omega_i \chi^{(3)} I_p L)^2}{4 n_i n_s n_p{}^2 c^4 \varepsilon_0{}^2} G e^{-\alpha_i L}, \tag{2}$$

where $\chi^{(3)}$ is the third-order nonlinear susceptibility, G is the phase matching factor, ω_i is the idler frequency, L is the effective overlap length of the fields involved in the FWM process (here approximately equal to the film thickness), and $I_{i,s,p}$ refers to the idler, signal, and pump intensities, respectively, while the subscript "ext" denotes fields external to the film. T_i refers to the transmission coefficient from AZO to silica for the idler, calculated at signal wavelengths, while $T_{s,p}$ is the transmission coefficient from AZO to silica for signal and idler wavelengths, respectively. We can reach the above equation through analytical treatment of semi-degenerate coupled-wave formalism where the attenuation coefficients for idler, signal, and pump waves are indicated by $\alpha_{i,s,p}$, and the momentum mismatch $\vec{\Delta}k = \vec{2}k_p - \vec{k}_p - \vec{k}_s$ is automatically satisfied in the thin-film condition. Considering negligible the attenuation at the idler frequencies and recording the output idler at the emission angle, the phase matching factor G, Eq. (3), reduces to a function of film thickness and attenuation factors alone

$$G = \frac{4\left(1 - \exp\left(\frac{-(\alpha_s + 2\alpha_p)L}{2}\right)\right)^2}{\left(\frac{(\alpha_s + 2\alpha_p)L}{2}\right)^2}. \tag{3}$$

As we can see by comparing the numerical and experimental data in Fig. 4, the general trend of the FWM conversion process is well explained by our considerations. The fit in Fig. 4 was achieved with a value of $\chi^{(3)} = 0.91 \times 10^{-20} \frac{\text{m}^2}{\text{V}^2}$. This value is very close to the one reported in [6], which ranges from $1.5 \times 10^{-20} \frac{\text{m}^2}{\text{V}^2} - 9.5 \times 10^{-20} \frac{\text{m}^2}{\text{V}^2}$. A justification for the monotonic behavior of the efficiency can be established by considering the reflectivity at the air AZO interface, which drops off as the signal wavelength is reduced, thus increasing the optical power available for FWM. The inset of Fig. 4 shows the plot of measured idler power versus increasing values of pump power squared. The almost linear trend demonstrates that the FWM process was correctly identified. No sign of saturation was detected within the covered power range.

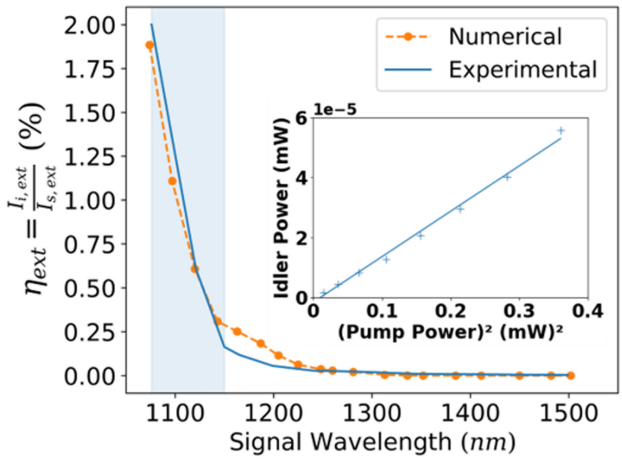

Fig. 4. Nonlinear conversion efficiency for the FWM process as a function of the signal wavelength. Due to the threshold-like behavior, an effective tunability range can be identified within which idler photon generation is more efficient (blue area). (a) Idler power versus pump power squared. As expected from the energy conservation diagram pertaining to the FWM process, the power of the converted signal (idler) follows a linear behavior regarding the pump power squared.

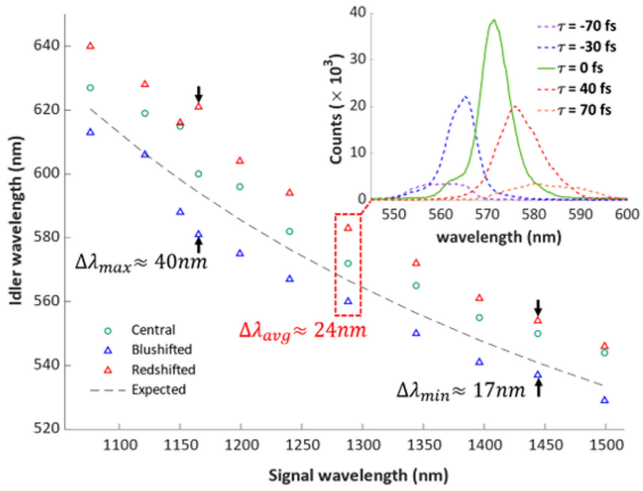

Fig. 5. Idler tunability range (via temporal synchronization) as a function of the signal wavelength. For a given signal wavelength, a triplet of points is provided indicating the wavelength peak location at $\tau = 0$ and for the adjacent spectra. Across the entire tunability range of the OPA, a wavelength shift of 24 nm in average is recorded for the idler spectra. "Expected curve" is calculated from energy conservation. The dashed red box highlights a data set reported in further detail in the inset. Inset shows idler spectra as a function of signal-to-pump delay τ. $\tau = 0$ indicates the temporal location for which maximum idler power is recorded at the spectrometer. The two curves adjacent to the central peak are recorded for the time delays at which the count rate at the spectrometer is half the maximum.

The remarkable time gradient of the signal index due to the intense pump can also be used to tune the idler wavelength by simply operating on τ [42,43]. This is shown in the inset of Fig. 5, where five different idler spectra are displayed for various pump-to-signal delays. We chose to indicate with $\tau = 0$ the temporal delay maximizing idler power. By collecting the

wavelength peak positions as a function of the signal wavelength at $\tau = 0$ and at τ such that the total counts are $1/2$ the $\tau = 0$ value we can plot the main graph, which shows how, by simply operating on the time delay, the idler spectrum can be tuned by more than its bandwidth (7 nm) across the entire tunability range of the OPA (experimental points within the red dashed box correspond to the spectra in Fig. 5 inset).

The results reported in the present Letter set a favorable condition for visible photon production via FWM in AZO's NZI region. The recorded signal-to-idler conversion efficiency reaches 2% in the investigated spectral region, with the possibility of higher efficiencies at shorter (longer) signal (idler) wavelengths. It is worth mentioning that the material's refractive index is still well below unity ($n \cong 0.5$) for the signal wave at the edge of the tunability range ($\lambda = 1050$ nm). This behavior is compatible with our analysis, which accounts for both reflectivity and material absorption. In addition to this, we also demonstrate that the temporal index profile, induced by an intense pump signal, can be judiciously exploited for tuning the idler wavelength in a pump/probe configuration. In this regard, by changing the mutual time delay between pump and signal, an average frequency shift of about 24 nm is attained on the central idler wavelength. This result extends our knowledge of NZI nonlinearities and the possibility of exploiting TCOs for tunable integrated visible sources.

Funding. Air Force Office of Scientific Research (FA9550-18-1-0002); Engineering and Physical Sciences Research Council (EP/P005446/1); Division of Materials Research (DE-SC0017717); Office of Naval Research (N00014-20-1-2199); Carnegie Trust for the Universities of Scotland (RIG009891); UK Research and Innovation (EP/S001573/1).

Disclosures. The authors declare no conflicts of interest.

Data Availability. Data underlying the results presented in this Letter are available in [44].

REFERENCES

1. G. P. Agrawal, *Fiber-Optic Communication Systems*, 4th ed. (Wiley, 2010).
2. J. Wang, F. Sciarrino, A. Laing, and M. G. Thompson, Nat. Photonics **14**, 273 (2020).
3. N. Kinsey, C. De Vault, A. Boltasseva, and V. M. Shalaev, Nat. Rev. Mater. **4**, 742 (2019).
4. O. Reshef, I. De Leon, M. Z. Alam, and R. W. Boyd, Nat. Rev. Mater. **4**, 535 (2019).
5. A. Klein, J. Am. Ceram. Soc. **96**, 331 (2013).
6. L. Caspani, R. P. M. Kaipurath, M. Clerici, M. Ferrera, T. Roger, J. Kim, N. Kinsey, M. Pietrzyk, A. Di Falco, V. M. Shalaev, A. Boltasseva, and D. Faccio, Phys. Rev. Lett. **116**, 233901 (2016).
7. E. G. Carnemolla, L. Caspani, C. DeVault, M. Clerici, S. Vezzoli, V. Bruno, V. M. Shalaev, D. Faccio, A. Boltasseva, and M. Ferrera, Opt. Mater. Express **8**, 3392 (2018).
8. A. Ciattoni, C. Rizza, and E. Palange, Phys. Rev. A **81**, 043839 (2010).
9. C. Argyropoulos, P.-Y. Chen, G. D'Aguanno, N. Engheta, and A. Alù, Phys. Rev. B **85**, 045129 (2012).
10. T. S. Luk, D. de Ceglia, S. Liu, G. A. Keeler, R. P. Prasankumar, M. A. Vincenti, M. Scalora, M. B. Sinclair, and S. Campione, Appl. Phys. Lett. **106**, 151103 (2015).
11. A. Capretti, Y. Wang, N. Engheta, and L. Dal Negro, Opt. Lett. **40**, 1500 (2015).
12. M. Z. Alam, I. De Leon, and W. B. Robert, Science **352**, 795 (2016).
13. O. Reshef, E. Giese, M. Z. Alam, I. De Leon, J. Upham, and R. W. Boyd, Opt. Lett. **42**, 3225 (2017).
14. J. B. Khurgin, M. Clerici, V. Bruno, L. Caspani, C. DeVault, J. Kim, A. Shaltout, A. Boltasseva, V. M. Shalaev, M. Ferrera, D. Faccio, and N. Kinsey, Optica **7**, 226 (2020).
15. J. B. Khurgin, M. Clerici, and N. Kinsey, Laser Photon. Rev. **15**, 2000291 (2021).
16. N. Kinsey and J. Khurgin, Opt. Mater. Express **9**, 2793 (2019).
17. R. Secondo, J. Khurgin, and N. Kinsey, Opt. Mater. Express **10**, 1545 (2020).
18. M. H. Javani and M. I. Stockman, Phys. Rev. Lett. **117**, 107404 (2016).
19. R. W. Boyd, J. Opt. Soc. Am. B **28**, A38 (2011).
20. N. E. Diego, M. Solís, and R. W. Boyd, arXiv:2008.10512 (2020).
21. H. Galinski, G. Favraud, H. Dong, J. S. T. Gongora, G. Favaro, M. Döbeli, R. Spolenak, A. Fratalocchi, and F. Capasso, Light Sci. Appl. **6**, e16233 (2017).
22. J. Wu, Z. T. Xie, Y. Sha, H. Y. Fu, and Q. Li, Photon. Res. **9**, 1616 (2021).
23. Y. Tian, F. P. García de Arquer, C.-T. Dinh, G. Favraud, M. Bonifazi, J. Li, M. Liu, X. Zhang, X. Zheng, M. G. Kibria, S. Hoogland, D. Sinton, E. H. Sargent, and A. Fratalocchi, Adv. Mater. **29**, 1701165 (2017).
24. I. Liberal and N. Engheta, Nat. Photonics **11**, 149 (2017).
25. P. Mao, C. Liu, G. Favraud, Q. Chen, M. Han, A. Fratalocchi, and S. Zhang, Nat. Commun. **9**, 5428 (2018).
26. N. Kinsey, C. DeVault, J. Kim, M. Ferrera, V. M. Shalaev, and A. Boltasseva, Optica **2**, 616 (2015).
27. M. Clerici, N. Kinsey, C. DeVault, J. Kim, E. G. Carnemolla, L. Caspani, A. Shaltout, D. Faccio, V. Shalaev, A. Boltasseva, and M. Ferrera, Nat. Commun. **8**, 15829 (2017).
28. Z. Fusco, M. Taheri, R. Bo, T. Tran-Phu, H. Chen, X. Guo, Y. Zhu, T. Tsuzuki, T. P. White, and A. Tricoli, Nano Lett. **20**, 3970 (2020).
29. L. Braic, N. Vasilantonakis, A. Mihai, I. J. Villar Garcia, S. Fearn, B. Zou, N. M. Alford, B. Doiron, R. F. Oulton, S. A. Maier, A. V. Zayats, and P. K. Petrov, ACS Appl. Mater. Interfaces **9**, 29857 (2017).
30. Y. U. Lee, E. Garoni, H. Kita, K. Kamada, B. H. Woo, Y. C. Jun, S. M. Chae, H. J. Kim, K. J. Lee, S. Yoon, E. Choi, F. Mathevet, I. Ozerov, J. C. Ribierre, J. W. Wu, and A. D'Aléo, Adv. Opt. Mater. **6**, 1701400 (2018).
31. R. W. Boyd, *Nonlinear Optics* (Academic, 2020).
32. M. Ferrera, L. Razzari, D. Duchesne, R. Morandotti, Z. Yang, M. Liscidini, J. Sipe, S. Chu, B. Little, and D. Moss, Nat. Photonics **2**, 737 (2008).
33. L. N. Quan, B. P. Rand, R. H. Friend, S. G. Mhaisalkar, T.-W. Lee, and E. H. Sargent, Chem. Rev. **119**, 7444 (2019).
34. J. Kim, G. V. Naik, N. K. Emani, U. Guler, and A. Boltasseva, IEEE J. Sel. Top. Quantum Electron. **19**, 4601907 (2013).
35. G. V. Naik, J. Kim, and A. Boltasseva, Opt. Mater. Express **1**, 1090 (2011).
36. M. Noginov, L. Gu, J. Livenere, G. Zhu, A. Pradhan, R. Mundle, M. Bahoura, Y. A. Barnakov, and V. Podolskiy, Appl. Phys. Lett. **99**, 021101 (2011).
37. E. Shkondin, O. Takayama, M. A. Panah, P. Liu, P. V. Larsen, M. D. Mar, F. Jensen, and A. Lavrinenko, Opt. Mater. Express **7**, 1606 (2017).
38. B. Yang, C. Yao, Y. Yu, Z. Li, and X. Wang, Sci. Rep. **7**, 1 (2017).
39. Z. L. Wang and J. Song, Science **312**, 242 (2006).
40. T. Williams, D. Hunter, A. Pradhan, and I. Kityk, Appl. Phys. Lett. **89**, 043116 (2006).
41. S. Song, C. T. Allen, K. R. Demarest, and R. Hui, J. Lightwave Technol. **17**, 2285 (1999).
42. V. Bruno, S. Vezzoli, C. DeVault, E. Carnemolla, M. Ferrera, A. Boltasseva, V. M. Shalaev, D. Faccio, and M. Clerici, Appl. Sci. **10**, 1318 (2020).
43. Y. Zhou, M. Z. Alam, M. Karimi, J. Upham, O. Reshef, C. Liu, A. E. Willner, and R. W. Boyd, Nat. Commun. **11**, 1 (2020).
44. M. Ferrera, E. G. Carnemolla, and W. Jaffray, "Dependence of the nonlinear-optical response of materials on their linear ε and μ," Heriot-Watt University, 13 September 2021, https://doi.org/10.17861/230a1677-efb9-42b0-afb1-a950e705a259.